

8 PULSE LENGTH MEASUREMENT

8.1 Autocorrelator Measurement

The pulse length is an important property of the HGHG radiation pulse (in addition to its energy and spectrum). In order to measure the pulse length of the HGHG output we attempted to use a commercial autocorrelator from Femtochrome Inc. While we did not succeed to carry out the measurement with the commercial device, it was instructive to work with it, leading to a design of a new autocorrelator, which worked perfectly.

8.1.1 Description of the Commercial Autocorrelator

The instrument is very compact, fitting in a framework of 16x32 cm. It has a beam splitter, two optical arms and a doubling crystal for the non-linear second harmonic generation. The layout of the autocorrelator is shown in box at the right hand side of Figure 8-1. One arm has a rotating mirror assembly, which may be used to vary the path length, however we use it as a fixed length arm. We change the delay by a micrometer attached to a roof-mirror in the other arm. The two arms are focused on the doubling crystal by a spherical mirror and produce the second harmonic generation (SHG) radiation. Following the SHG crystal the beams are reflected out to the detector. While compactness has its virtues, this autocorrelator is too limited in space. The entrance and exit ports are close to each other. There is only enough space for the detector but not enough space to move the detector for each arm. Thus we use a lens system to collect all arms into the detector. The spherical mirror also reflects the two beams down to the crystal, thus the beams upstream of spherical mirror are only 5 mm above the crystal, restricting our ability to make adjustments.

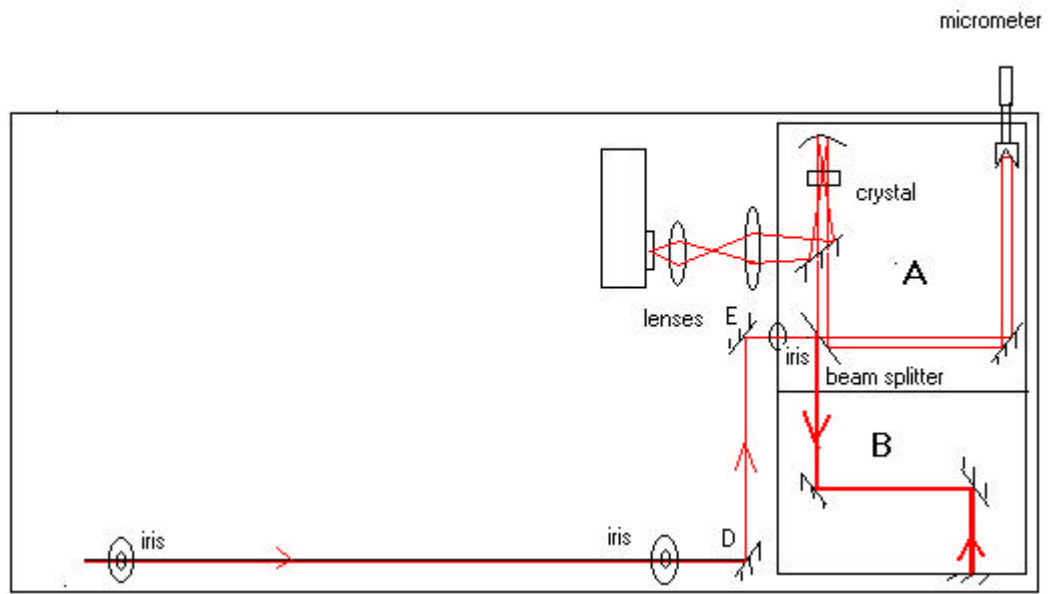


Figure 8-1 The commercial autocorrelator layout

The beam splitter of the autocorrelator was a 3 mm thick Zn-Se. We tested various crystals to be used for doubling the 5.3 μm beam.

8.1.2 Tests of the AgGaS₂ Harmonic Generation Crystal

The Figure 8-2 describes the non-linear second harmonic generation of 5.3 μm pulse in a crystal.

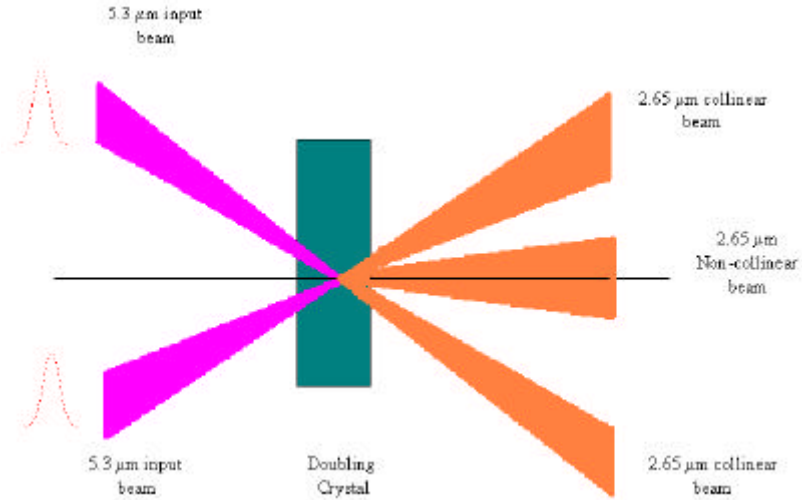


Figure 8-2 Second harmonic generation using a doubling crystal

The first crystal to be tested was a AgGaS₂ crystal, borrowed from the BNL Chemistry Department. The 5.3 μm radiation for the test was obtained from a AgGaSe₂ crystal, doubling the 10.6 μm CO₂ laser. Then the AgGaS₂ crystal under test doubled the 5.3 μm light to 2.65 μm . (See Figure 8-3).

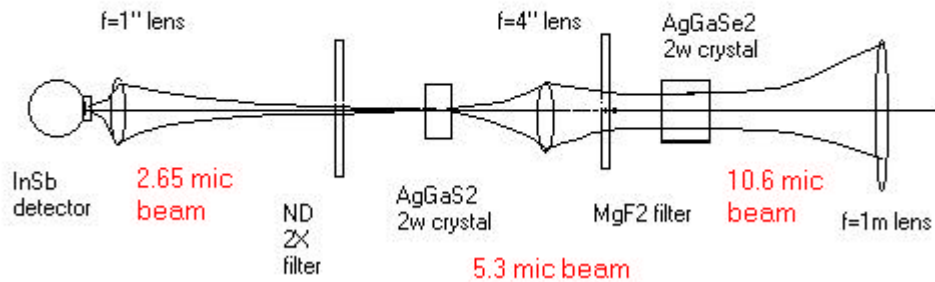


Figure 8-3 Crystal Testing Setup

We focused the 10.6 μm beam near the AgGaSe_2 crystal to get high conversion efficiency, but avoided focusing exactly on the crystal not to damage. We focused the 5.3 μm beam on the second test crystal using a 4-inch focal length lens.

The MgF_2 filter is used to block the 10.6 μm beam from reaching the AgGaS_2 crystal, and an ND filter is used to block the 5.3 μm to make sure that we are measuring only the 2.65 μm light.

The CO_2 laser energy was 100 mJ and the 5.3 μm was in the range of 200-300 μJ . At 2.65 μm we observed a large fluctuation (100%) and the peak signal was about 3 Volts with 2X attenuation. This corresponds to 150pJ energy. The beam size on the crystal was 1.5 mm diameter.

8.1.3 Polarization and the Acceptance Angle in the Crystal Test Setup

We started with a horizontally polarized beam, which was rotated 90° to the vertical using a wave-plate placed before the first crystal. The polarization is rotated by 90° at crystal during the doubling process and becomes horizontal again.

At the test crystal, the FWHM vertical angular acceptance is 30 mrad, which is 1.7° . The horizontal acceptance is about 10° .

8.1.4 Testing of the LiIO_3 Harmonic Generation Crystal

The LiIO_3 crystal came with the autocorrelator, mounted in the original holder. Without disturbing the above mentioned test set-up we replaced AgGaS_2 crystal with LiIO_3 and repeated the measurements. We got around 2.5 Volts signal with In-Sb detector. Therefore we concluded that this crystal is as good as the AgGaS_2 crystal and decided to stay with the original LiIO_3 crystal.

8.1.5 Autocorrelator Tests

In order to test the autocorrelator we used a frequency doubled CO_2 laser. We started with the oscillator beam, which has a 75 ns pulse length. This long pulse length beam should allow us to spatially align the autocorrelator without worrying about the

temporal synchronization of the two arms of the autocorrelator. This test has failed because of the noise problem in the CO₂ oscillator room.

Following that failed test, we decided to test the autocorrelator by amplified CO₂ laser. The amplified CO₂ laser beam has a power about several GW and a pulse length of 200 ps. We set the autocorrelator in the terawatt laser room, which is less noisy. Since the amplifier has much more power, we were concerned about the damage threshold of the crystals. The threshold power density for the crystal is about 100 MW/cm². We measured the 10.6 μm CO₂ laser energy as 10-20 mJ and the beam size was 1.5 cm diameter. Thus the intensity was about 50 MW/cm², and it was safe to use the whole beam without using any attenuators. We measured 2.5 μJ energy at 5.3 μm wavelength. For this energy we still did not have any problem with damaging the second crystal in the autocorrelator even though the beam size is about a millimeter.

We noticed that there is a quite large misalignment between the 5.3 μm beam and He-Ne alignment laser. The separation between the two 5.3 μm beams before the spherical mirror in Figure 8-1 was about 2-3 mm whereas the He-Ne laser separation was about 5-6 mm. We realized that the beam splitter has some wedge and thus produces chromaticity, which causes the misalignment. We took the beam splitter out and characterized it.

8.1.6 Beam Splitter Test

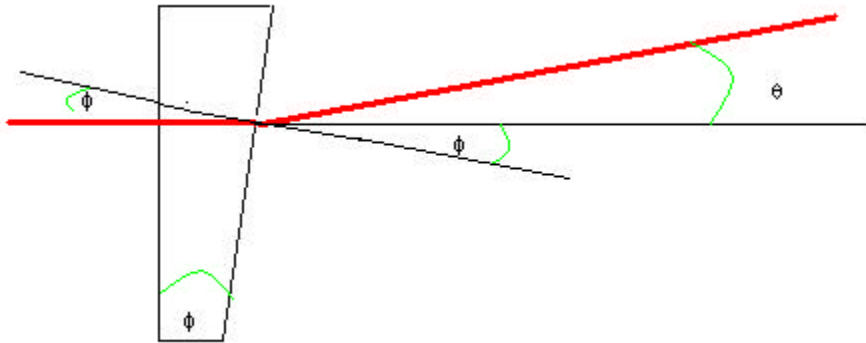


Figure 8-4 Wedge geometry of a beam splitter

When we put the beam splitter normal to the beam as shown in Figure 8-4 we measured a deflection of $\theta=9.3\text{mrad}$. Using Snell's law

$$n_1 \sin q_1 = n_2 \sin q \quad \text{Eqn 8-1}$$

For Zn-Se the index is 2.65 for He-Ne.

Assuming small angles

$$n \sin f = \sin(q + f) \quad \text{Eqn 8-2}$$

$$nf = q + f \quad \text{Eqn 8-3}$$

Therefore

$$f = \frac{q}{n-1} \quad \text{Eqn 8-4}$$

resulting $f = 5.6 \text{ mrad}$

We repeated the same measurement at $5.3 \mu\text{m}$ and got an angle of 5.8 mrad . The index of refraction of Zn-Se at $5.3 \mu\text{m}$ is 2.45.

During the characterization of the beam splitter, we also noticed that the He-Ne reflecting from the surface B is weak but He-Ne reflecting from the surface A is strong as shown in Figure 8-5. The $5.3 \mu\text{m}$ light is reflecting at the same surface as strong He-Ne is reflecting. Since He-Ne laser is the reference for alignment it is important to know which beam to follow.

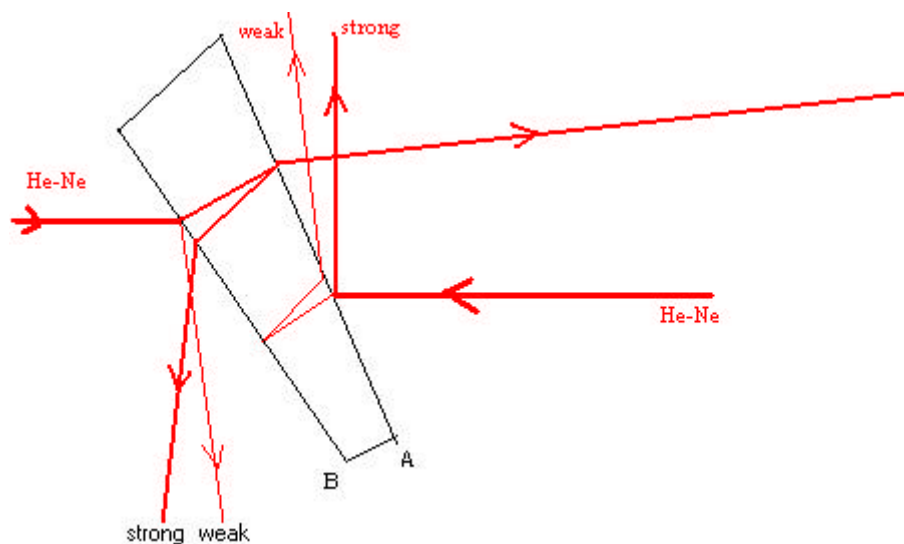


Figure 8-5 Beam Splitter Reflection Properties

8.1.7 The Autocorrelator Test with 3.2 μm Laser

We decided to test the autocorrelator at Laser Lab in Chemistry Department using 3.2 μm laser. The advantages of this laser are a high repetition rate ($\sim\text{kHz}$) and its visibility on a liquid crystal card.

We moved the autocorrelator to Laser Lab in Chemistry department and aligned it. We realized that the 3.2 μm laser reflects from surface B of the beam splitter whereas the He-Ne light and the 5.3 μm light are reflecting from surface A.

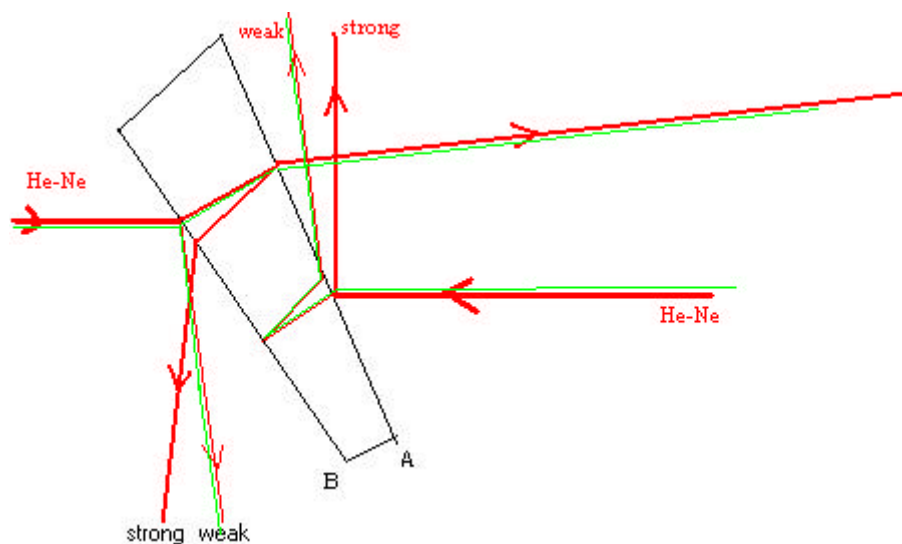


Figure 8-6 Beam Splitter Reflection Properties

The green line in Figure 8-6 indicates the 3.2 μm laser. Thus following the weak He-Ne we were able to align the autocorrelator.

Since the chromaticities of the He-Ne laser and the 3.2 μm laser are closer as compared to 5.3 μm , alignment was easier and we were able to measure the autocorrelation full width divided by the square root of 2 as 3.6 ps. The expected FWHM value is supposed to be 1.5-2ps, in reasonably close agreement.

The success of this measurement is also due to the characteristics of the crystal at 3.2 μm wavelength. The acceptance angle is so small such that we were able to measure only one arm (collinear or non-collinear) at a time. This makes the signal to noise ratio much better than in the 5.3 μm measurements, where the larger angular acceptance allows contamination from the collinear beams.

8.1.8 The New Autocorrelator Design

Having gained a better understanding of the limitations of the commercial autocorrelator, we decided to build a new autocorrelator. This new device will be equipped with a flat Zn-Se beam splitter and a special AgGaSe₂ crystal, designed for 5.3 μm . We designed the autocorrelator to be simpler and spacious. In the commercial autocorrelator there were two lenses at the exit port to transport the beam to the detector. In the new design we eliminated these lenses. Since we expected a fairly strong HGHG

signal at the detector we did not mind expanding the beams and collecting only a small fraction, the size of the detector sensitive area. The layout of the autocorrelator is shown in Figure 8-7.

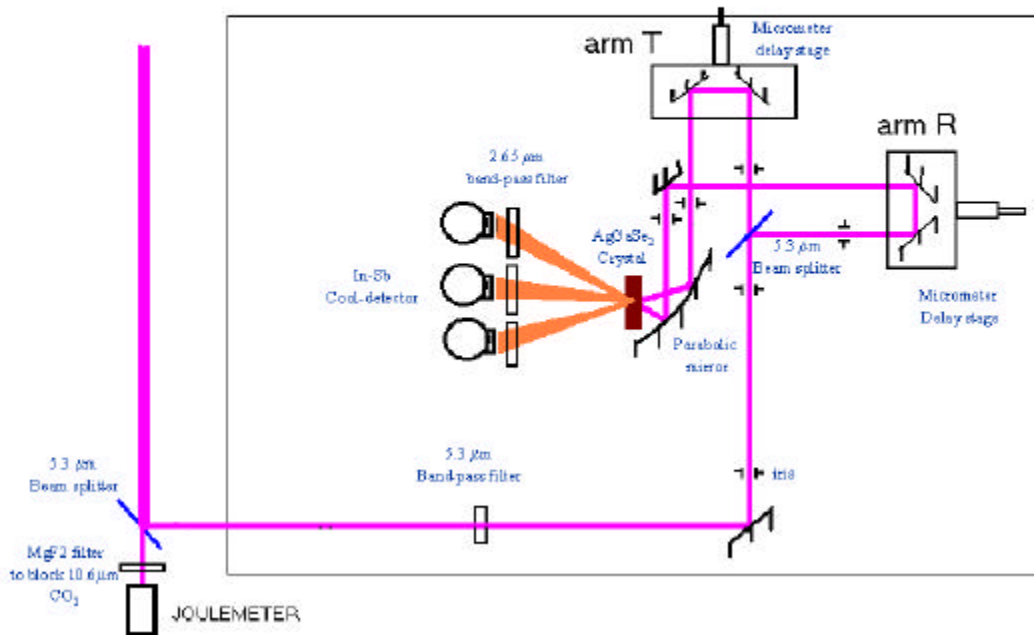


Figure 8-7 The new autocorrelator layout

The 5.3 μm light is split and part of it goes to the joulemeter [12] for normalization purposes. The other part goes into the autocorrelator. We use a 5.3 μm wavelength band-pass filter to block the 10.6 μm contamination from the CO₂ laser. Two irises upstream of the beam splitter are used as an alignment reference. Both arms have micrometer delay stages for convenience. There are four irises between the beam splitter and the parabolic mirror to control internal alignment. Each delay micrometer stage is positioned on an individual stage, which can move in perpendicular direction enabling to change the separation between the beams upstream of the parabolic mirror. We would like to separate these two beams as much as possible because a larger separation provides more divergence and therefore a better signal to noise ratio. The 1-inch focal length parabolic mirror is used to focus the beams onto the crystal. The beam size in the crystal is less

than 300 μm . The crystal is positioned on a rotating stage (enabling us to change the angle) and seated on a micrometer stage (allowing us to find the focus position precisely). The In-Sb detector is located on a micrometer stage where the 2.65 μm beams are about 6 mm in diameter. This micrometer stage allows us to move the detector between the non-collinear and collinear beams, allowing us choose the arm that we want to measure (see Figure 8-7). A 2.65 μm wavelength band-pass filter is located in front of the detector to block the 5.3 μm wavelength light.

8.1.9 AgGaSe₂ Crystal Test

We ordered a new $5 \times 5 \times 1 \text{ mm}^3$ AgGaSe₂ crystal. The group velocity mismatch 48 fs/mm [43] and geometric beam overlap in the crystal allow better than 0.5-ps resolution. When we received the crystal we characterized it before installation in the autocorrelator. We used the same set up shown in Figure 8-3. During this test we had 80 mJ of CO₂ laser signal and 70 μJ of the doubled 5.3 μm signal. At 2.65 μm we measured several volts using a 1000X attenuation, which corresponds to about a 100 nJ. This means that the conversion efficiency is about 10^{-3} . This efficiency is 3 orders of magnitude better than the efficiency of the LiIO₃ crystal. The measured the horizontal acceptance angle at about 10°. In the vertical direction the signal is not sensitive to rotation therefore the acceptance angle is pretty large.

8.1.10 Testing the Autocorrelator with 1.064 mm Nd:YAG Laser

Before we use the new autocorrelator with the HGHG beam, we wanted to test it with a known laser source to determine the zero position of the two arms and study its operational characteristics. With the slow repetition rate of the CO₂ laser (15 seconds), finding the zero position is time consuming.

We decided to use the ATF's 1.064 μm Nd:YAG laser. We set up the autocorrelator in the laser laboratory. A BBO crystal was used as the doubling crystal. We started measuring the individual arms and determined the crystal angles appropriate

for this wavelength. The doubled beam's wavelength is 532 nm, which is green light. Thus it is measurable on a CCD camera and even strong enough to observe by eye. Using the CCD camera we checked the co-alignment of local He-Ne laser and the doubled beams. The overlap was very good.

Then we set the crystal angle to middle of the two arms and then moved the delay arm to catch the non-collinear beam. We optimized the crystal position by maximizing the signal. A photo-diode detector is used to measure the green lights. We scanned the delay arm and obtained the autocorrelation curve shown in Figure 8-8. The blue curve is the Gaussian fit to the data. The FWHM of the curve is 3.2 mm.

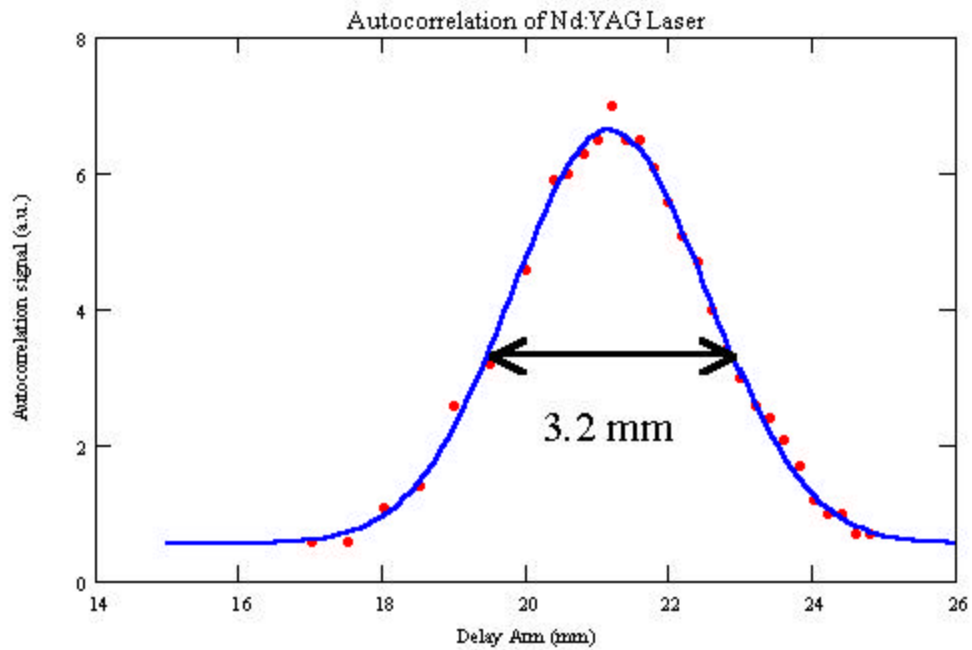


Figure 8-8 The Autocorrelation curve of the Nd:YAG Laser

When two beams are interacting to produce higher harmonic in a crystal, the pulse length broadens because of the convolution. Assuming temporal pulse shape is $f(t)$ where t is the time, the convolution integral will be

$$G(t) = \int f(t') * f(t - t') dt' \quad \text{Eqn 8-5}$$

Thus the FWHM of the convolution $G(t)$ is larger than the FWHM of function $f(t)$ by some factor. The broadening factor depends on the pulse shape $f(t)$. If the pulse

shape is a Gaussian then the broadening factor will be $\sqrt{2}$. If the pulse shape is Lorentzian then the broadening factor will be 2.

For this measurement we assume that the pulse shape is a Gaussian. A feature of the set-up is that a 1 mm movement on one of the delay arms corresponds to a 2 mm actual delay, or 6.6 ps in time. Thus the measured 3.2 mm is equivalent to pulse length of 15 ps. The pulse length of the Nd:YAG laser was previously measured (using a streak camera) to be 14-15 ps. This is a very good agreement.

As a result of this measurement we confirmed that spatial alignment of the autocorrelator and determined the zero position of the two arms and the crystal position to be used in the HGHG autocorrelation measurement.

8.1.11 Measuring The Pulse Length Of The HGHG Output

After testing the autocorrelator with the Nd:YAG laser successfully we proceeded to measure the pulse length of the HGHG output.

We aligned the autocorrelator using a local He-Ne laser. The beam-line He-Ne laser is also co-aligned with the local He-Ne. Since the beam-line He-Ne is well co-aligned with the HGHG radiation we establish a good alignment in the autocorrelator. As a first step in measuring the wiggler radiation, we checked the alignment with the SASE signal. We removed the 2.65 μm band-pass filter and measured the SASE signal coming from the collinear arms. The SASE signal intensity relative to the normal signal is reduced for two reasons. First, the detector is collecting only a 1 mm diameter portion of the 6 mm diameter beam. Second, the signal is split into two arms. We verified the position of the detector by observing the maximum signal position and find that it is very consistent with the He-Ne laser position.

Then we switched to the HGHG case. We placed the 2.65 μm band-pass filter back in front of the detector. We adjusted the crystal angle for each arm by looking at the back reflection of the He-Ne laser. The bisector of the angle formed by the collinear beams is where we should look for the non-collinear arm.

In the next step we measured the collinear HGHG signals and noted the signal strength in the doubled frequency. Then we pointed the crystal at the non-collinear beam.

The noise level is measured by blocking one arm at a time. We got about 100 mV noise contamination from arm R and about 50 mV from arm T (see Figure 8-7). Then we unblocked both arms to measure the non-collinear beam. Since the zero position of the delay arms was known from the Nd:YAG laser test, we got the signal from the autocorrelation immediately. The maximum signal that we obtained for a full temporal overlap was about 1.2 V. thus the signal to noise ratio is about 10 to 1.

We scanned the delay arm R and recorded the autocorrelator signal and split HGHG signal for normalization. The doubling efficiency is proportional to the square of the input intensity. Thus to normalize the measurement we divided the autocorrelator signal by the square of the HGHG output as measured by the joulemeter.

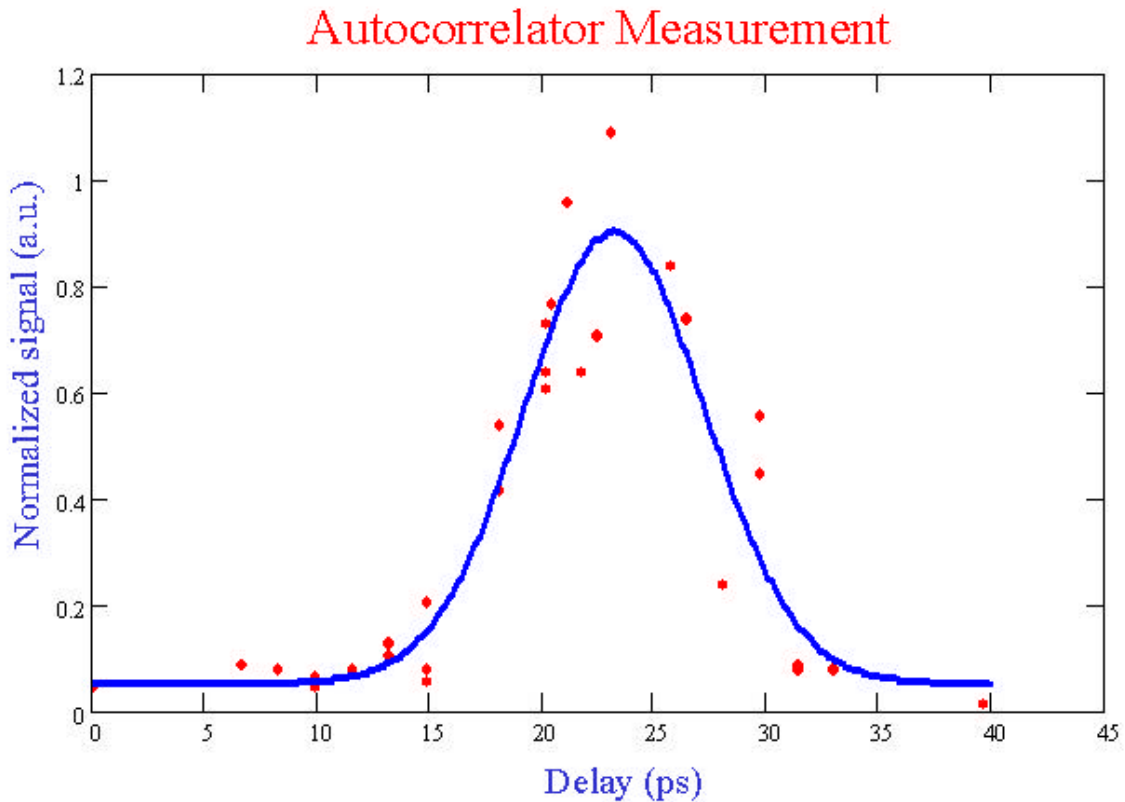


Figure 8-9 The Autocorrelation curve of the HGHG Output

The normalized signal vs. time-delay and the Gaussian fit is shown in Figure 8-9 [44]. Here we assume that the HGHG pulse shape is a Gaussian. The FWHM of the autocorrelation curve is 8.4 ± 0.5 ps. Thus the HGHG pulse length is then 5.9 ± 0.4 ps.

The measured electron beam pulse length is 6 ps. (See Figure 8-10)

Peak current [amps]: $I_{\text{peak}} = 129.3$

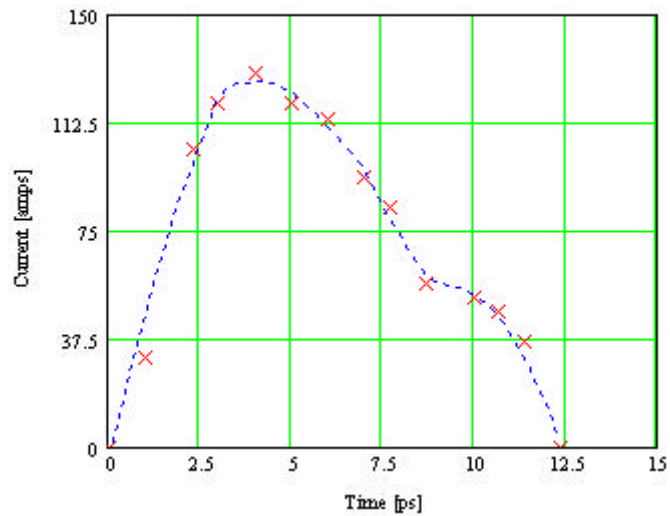


Figure 8-10 Electron beam longitudinal pulse shape

These results will be discussed later.

8.2 Coherence Length Measurement Using The Michelson Interferometer

The Michelson interferometer can be used to measure the coherence pulse length of a laser beam. The classical Michelson Interferometer produces interference fringes on the exit screen (as shown in Figure 8-11) as long as the two arms overlaps within a coherence length.

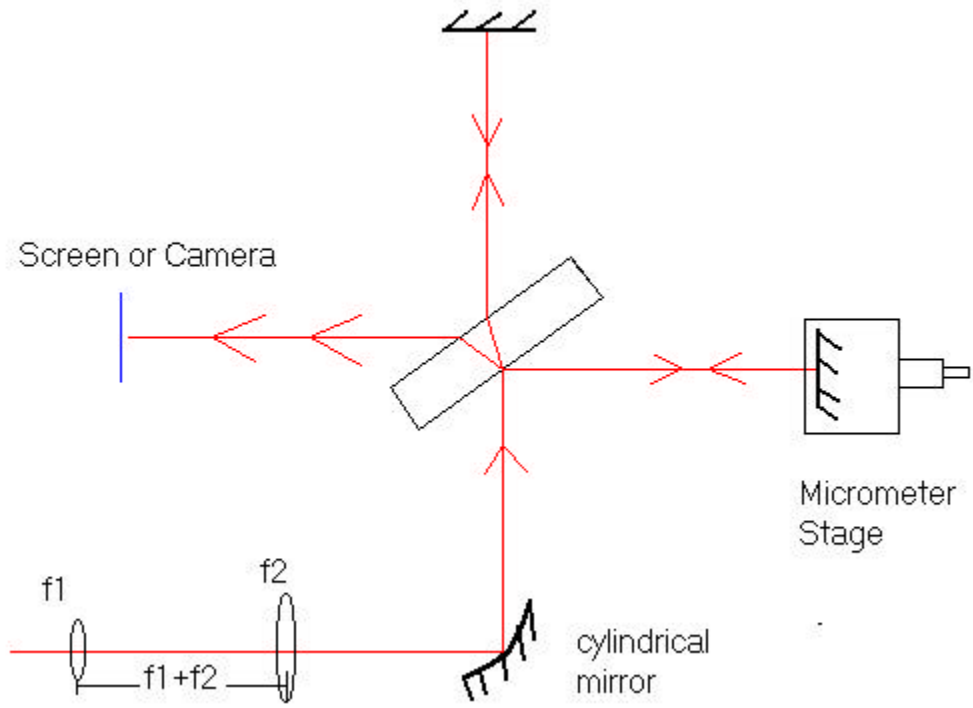


Figure 8-11 Michelson Interferometer

The fringes go from a constructive interference to destructive interference and then back to constructive interference within a delay mirror movement of $I/2$ (the pathlength difference of I). The typical plot of intensity versus delay is shown in Figure 8-12 [45].

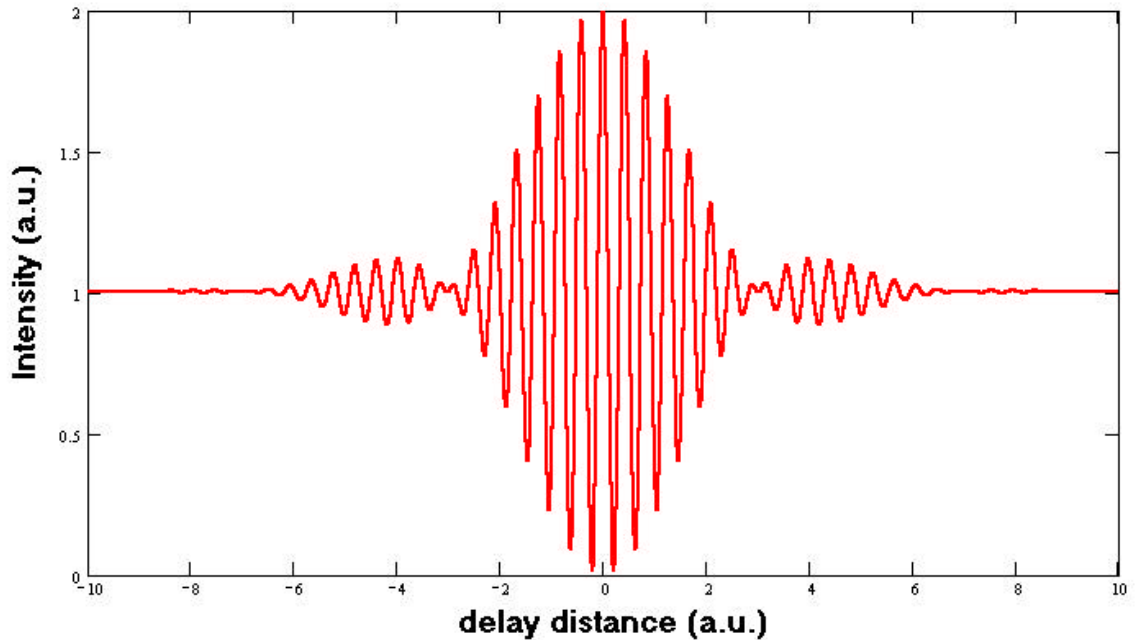


Figure 8-12 Intensity vs. delay distance (interferogram)

The rapid oscillation of intensity gradually tapers in an envelope function because of a finite bandwidth of the source. As we move along the pulse the phase shift slightly varies for different wavelengths within the bandwidth. Thus the amplitude of the fast intensity fluctuation reduces as the delay increases.

By measuring the maximum and minimum intensity of the fringes at each delay positions it is possible to map the envelope function.

Michelson has introduced the notion of “visibility” as $\frac{I_{\max} - I_{\min}}{I_{\max} + I_{\min}}$. This technique

is a multi-shot measurement similar to the autocorrelator technique that we used in the previous section. However the difference between the autocorrelator and the interferometer measurements is critical. The autocorrelator measures the intensity pulse length of the beam. On the other hand the interferometer measures the coherence length of the beam.

The HGHG output is strong enough to be seen by the pyroviewer infrared camera, with enough power to spare on interferometer losses. This is a convenient diagnostic, thus we decided to use a Michelson interferometer with the pyroviewer and the sensing element as a comparison to the autocorrelation technique. In order to see as many fringes

as possible on the camera we used a telescope to expand the beam to fill the camera. Since this expansion is necessary only in one linear axis, and we do not want to lose intensity, we used a cylindrical mirror. Thus we obtained a focused image in one axis and an expanded image on the other axis. (See Figure 8-11)

Having obtained a vertical interference pattern in the camera, we scanned the delay arm and recorded the interference fringe patterns as a function of delay. Sample patterns are shown in Figure 8-13.

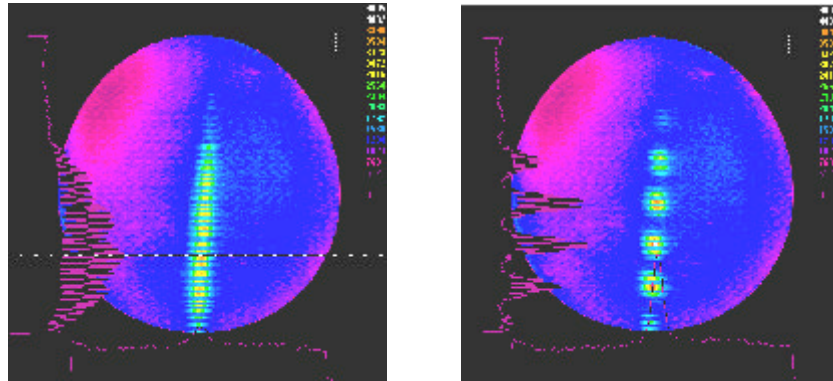


Figure 8-13 (a) & (b) Interference Patterns

Figure 8-13 (a) shows the pattern when the two pulses starts overlapping and Figure 8-13 (b) shows when they are fully overlapped. After recording the images of the fringe patterns we measured the visibility of the fringes. We define the visibility as follows:

$$Visibility = \frac{(\max_of_the_peak - \min_of_the_dip)}{(\max_of_the_peak + \min_of_the_dip)}$$

The denominator is for normalization purpose. The plot of the visibility as a function of delay arm is as shown in Figure 8-14.

Interferometer Measurement

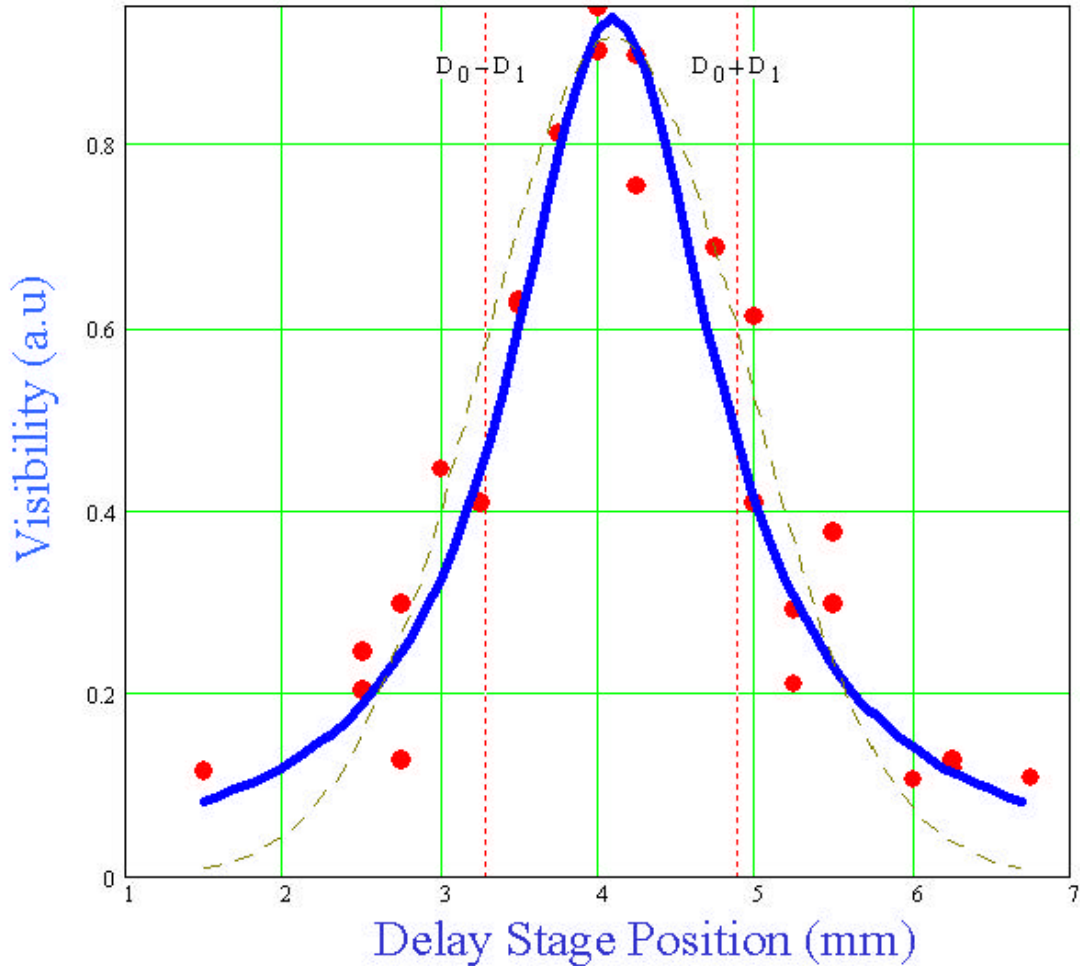


Figure 8-14 Michelson Interferometer Measurement

The blue curve is the Lorentzian fitting and brown dashed curve is Gaussian fitting to the data. D_0 is the peak position and $2D_1$ is the FWHM of the Lorentzian fit. The FWHM of the curve is 1.6 mm, which corresponds to 5.3 ps [44].

In conclusion, the FWHM coherence length is very close to the FWHM autocorrelation length, thus the HGHG output is practically fully coherent.